Carranza Castillo, O.; Figueres Amorós, E.; Garcerá Sanfeliú, G.; González Medina, R. (2013). Analysis of the control structure of wind energy generation systems based on a permanent magnet synchronous generator. Applied Energy. 103:522-538. doi:10.1016/j.apenergy.2012.10.015.

Analysis of the control structure of a wind generation system based on permanent magnet synchronous generator

O. Carranza[1,2], E. Figueres[2],G. Garcerá[2], R. Gonzalez-Medina[2]

[1]Escuela Superior de Cómputo, Instituto Politécnico Nacional,
Av. Juan de Dios Batiz S/N, Col. Lindavista, Del. Gustavo A. Madero,
07738, D.F., México, email *ocarranzac@ipn.mx,*

[2]Grupo de Sistemas Electrónicos Industriales, Departamento de Ingeniería Electrónica,
Universidad Politécnica de Valencia, Camino de Vera S/N, 7F, 46020,
Valencia, Spain*, http://www.gsei.upv.es, email: efiguere@eln.upv.es, ggarcera@eln.upv.es,*

Abstract

This paper presents the analysis of the two control structures used in wind generation systems with permanent magnet synchronous generators, variable speed and fixed pitch, to determine which structure is most appropriate for implementation. These control structures are speed control and torque control. The analysis considers all the elements of wind power generation system, with greater emphasis on the model of the turbine where mechanical torque is considered as a system variable and not as in other studies where it is considered as internal disturbance in the system. The analysis is developed so that the control structure is independent of AC/DC converter that is used in the system. From the analysis is obtained that the speed control can be stable using classical control techniques because it is a nonminimum phase system and the torque control is unstable because it has poles and zeros in the right half plane, very low frequency and very close to each other, so it is very difficult to control using classical control theory. In the evaluation of the speed control structure, the AC/DC converter is Three-phase rectifier Boost in Discontinuous Conduction Mode with an input filter and a Peak Current Control and to avoid the need of mechanical sensors, a Linear Kalman Filter has been chosen to estimate the generator speed.

1. Introduction

Wind Generation Systems (WGS) are currently taking a great interest in renewable energy systems [1]. This is mainly due to the high cost of fossil fuels and the need for clean energy sources. Although in the case of wind energy not all places are suitable for fully take advantage of this energy. Nevertheless, several statistical methods have been developed to calculate the average wind speed, the wind power density and its capacity factor for a specific geographical area [2]. Currently, there are numerous projects to implement wind energy farms increasing the production of clean electrical energy [3]. Several studies analyse the viability of wind energy, regarding both its generation capability to replace fossil energy, and the energy price reduction when introducing wind energy to satisfy the demand [4]. Furthermore, the administrations of many countries are establishing incentives and subsidies for those projects, in order to comply with the Kioto protocol about the reduction of CO_2 emissions. This fact makes that wind energy becomes cost-effective, competing with conventional generation of electricity.

Currently wind energy can be used under various schemes, that is, primary source with storage systems provide energy in remote locations [5]; as primary energy source with conventional sources to inject energy into a grid; and as an energy source in microgrids schemes in distributed generation systems [6]-[7].

In small power wind generation systems ranging from *1kW* to *50kW*, permanent magnet synchronous generators (PMSGs) are preferred to other electrical machines like induction generators (IGs) [8]-[10]. The reason of that is the need of IGs to be externally magnetized, so that they may be either directly connected to the grid or indirectly, by means of a back-to-back converter. In the first case, the speed regulation is limited up to around a 30% of the nominal IG speed [8], so that its capability of extracting energy from the wind is reduced. A back to back converter may be used to expand the IG speed range, improving the amount of energy that the

system can extract from the wind. Nevertheless, this topology is often too complex and expensive to be a good candidate for the low power range. On the contrary, PMSGs don't need an external magnetization, so that they are compatible with the use of passive rectifiers in cost effective grid decoupled systems. In addition, the use of a gearbox may be avoided, simplifying the mechanical structure of the system. PMSGs can work in grid isolated geographical zones and in a wide wind speed range, extracting a higher energy from the wind [10]-[11] than IGs.

Due to the fact that both the output voltage and the frequency of a PMSG depend on the wind speed, An AC/DC converter and a DC/AC converter (inverter) are required for connecting the generator to the grid. The inverter is responsible for regulating active and reactive power, which is injected to the grid, and it controls the voltage of the DC-Link. There are basically two types of configurations of converters used when it has a PMSG, the first type is an uncontrolled rectifier and a DC/DC converter and the other type is a controlled rectifier. The topology that uses the controlled rectifier and inverter, it is known as converter back-to-back.

One of the important points in wind power generation systems is to convert the most energy from wind power, seeking to achieve high levels of efficiency and quality of energy that is injected into the grid, which leads the implementation of control strategies that allow it [12]-[13]. For the case under study, where the WGS uses a PMSG, the system operates at variable speed and fixed pitch; the control structures are used control torque and speed control.

Note that in both cases there is a torque control through the generator output current, only in the case of torque control is straightforward and in the case of speed control is an indirect torque control through an intermediate stage that controls the generator speed [14]. The concept of torque control structure proposed in the SGE is shown in Fig. 1 and the concept of speed control structure proposed in the SGE is shown in Fig. 2. The MPPT block represents the algorithm of the maximum power point tracking that provides the reference current (I_{ref}) in the control structure of torque (current) or provides the speed reference (ω_{ref}) in the structure of the speed control , which is outside the scope in this paper.

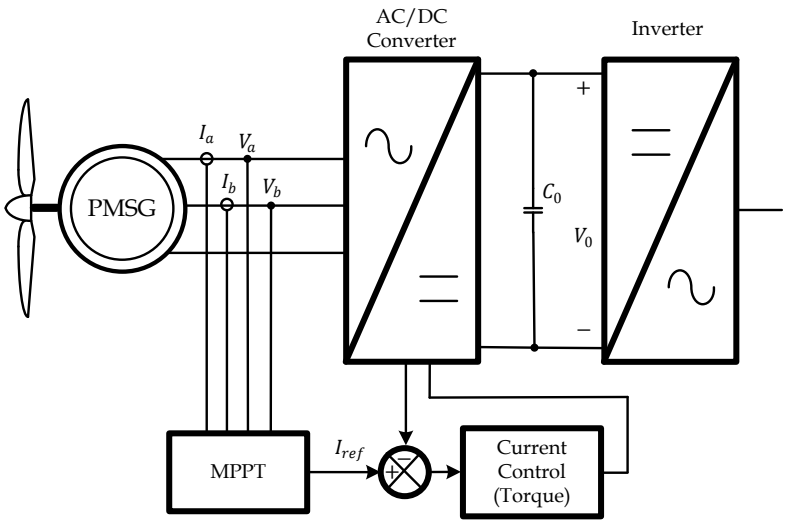

Fig. 1. Concept of torque control structure in the SGE proposed.

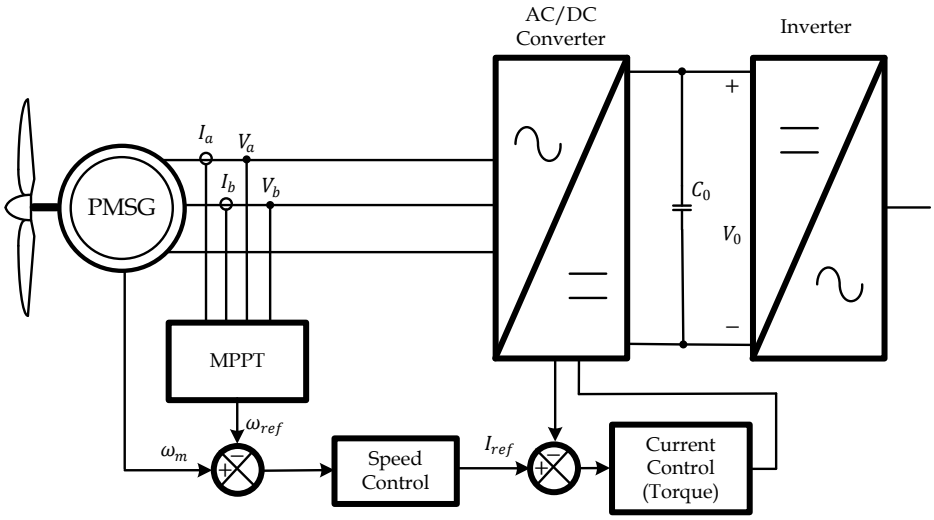

Fig. 2. Concept of speed control structure in the SGE proposed.

This paper is focused on the analysis both speed and torque control structures and design of the speed control loop of the system, which allows to have a stable system with a speed control structure. This confirms that the selected control structure is correct. The analysis is developed to consider all the variables of the system, mainly the mechanical torque, because most of the systems, it is considered an internal disturbance of the system to simplify the system. The analysis of the control structure is independent of the type of AD/DC converter which is used in the WGS, as well as the current control employee. To test the proper selection of the control structure, it is used three-phase boost rectifier working in DCM with LCL input filter as a AC/DC converter and a peak current mode control, both are described in [15]. This rectifier and current control provide a low total harmonics distortion current in PMSG and high power factor, in the speed range of the generator. Thus achieving increased system efficiency and reducing mechanical stress of the generator.

Table I shows the values of the parameters of the wind generation system.

Table I. Characteristics in the proposed WECS.

Characteristics	Values
Output power of the generator (P_o)	$2\ kW$
Output voltage range of the generator ($V_{ab} = V_{bc} = V_{ca}$)	$104\ -\ 416\ Vrms$
Constant of the electromotive force (K_{fem})	$0.9022\ Vpeak/rad/s$
Number of poles (n_p)	12
Speed range of the generator (n_m)	$150\ -600\ rpm$
Angular mechanical frequency range of the generator (ω_m).	$15.7 - 62.83\ rad/s$
Angular electrical frequency range of the generator (ω_e)	$94.2 - 376.98\ rad/s$
Inductance of one phase of the generator ($L_{ga} = L_{gb} = L_{gc}$)	$25\ mH$
Resistance of one phase of the generator ($R_{Lga} = R_{Lgb} = R_{Lgc}$)	$5\ \Omega$
Wind turbine coefficients	$a = 0.043, b = 0.108, c = 0.146$ $d = 0.0605, e = 0.0104, f = 0.0006$
Wind turbine ratio (r)	$1.525\ m$
Inertia Coefficient of the system (J)	$0.5\ kg\ m/\ s2$
Density of wind (ρ)	$1.08\ kg/m3$
DC link Capacitance (C_0)	$2\ mF$
DC link voltage (V_0)	$650\ V$
Sampling time (T_s)	$10\ \mu s$

2. Wind Turbine

2.1 Wind Turbine Model

The mechanical behavior of the wind turbine follows (1)

$$J\frac{d\omega_m}{dt} + B\omega_m = T_m - T_e \tag{1}$$

where J is inertia coefficient, B is the friction coefficient, ω_m is the turbine rotational speed, T_m is the turbine mechanical torque and T_e is the electrical torque applied to the PMSG rotor.

The mechanical power generated by the wind turbine (P_m) and T_m are expressed by equations (2) and (3), respectively.

$$P_m = \frac{1}{2}\rho\pi r^2 C_p(\lambda)V_\omega^3 \tag{2}$$

$$T_m = \frac{1}{2}\rho\pi r^3 C_t(\lambda)V_\omega^2 \tag{3}$$

where ρ is the density of the air, r is the wind turbine rotor radius, V_ω is the wind speed, $C_p(\lambda)$ is the power coefficient, $C_t(\lambda)$ is the torque coefficient. Both coefficients depend on the tip-speed-ratio parameter (λ), and it is expressed by (4).

$$\lambda = \frac{r\omega_m}{V_\omega} \tag{4}$$

$C_p(\lambda)$ is expressed by (5) and $C_t(\lambda)$ is expressed by (6). Fig. 3 shows both $C_p(\lambda)$ and $C_t(\lambda)$ characteristics as a function of the tip-speed ratio.

$$C_p(\lambda) = a + b\lambda + c\lambda^2 + d\lambda^3 + e\lambda^4 + f\lambda^5 \tag{5}$$

$$C_t(\lambda) = \frac{C_p(\lambda)}{\lambda} \tag{6}$$

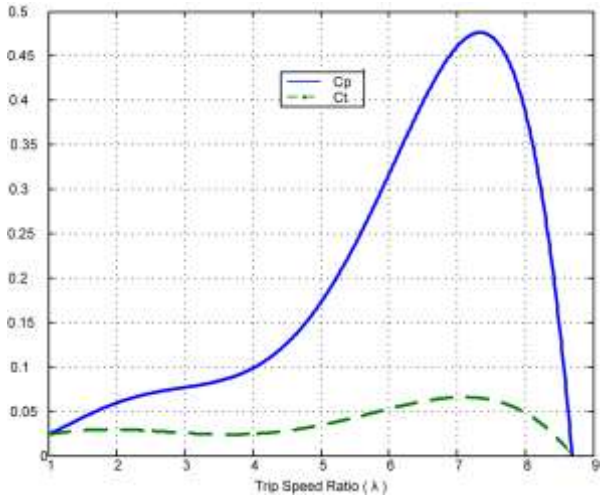

Fig. 3. Power and torque coefficients.

2.2 Permanent Magnet Synchronous Generators Model

The equivalent circuit of the permanent magnet synchronous generator [16] is shown in Fig. 4. Where $L_{ga} = L_{gb} = L_{gc}$ are the inductances of one phase, $R_{Lga} = R_{Lgb} = R_{Lgc}$ are the resistance in

series of one phase, V_a, V_b and V_c are the generator instantaneous output voltages and e_a, e_b and e_c are the electromotive forces, which are expressed by (7).

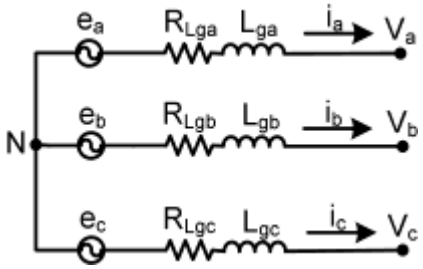

Fig. 4. Equivalent circuit of the permanent magnet synchronous generator.

$$\begin{aligned} e_a &= K_{emf}\omega_e \sin(\omega_e t) \\ e_b &= K_{emf}\omega_e \sin\left(\omega_e t - \frac{2\pi}{3}\right) \\ e_c &= K_{emf}\omega_e \sin\left(\omega_e t + \frac{2\pi}{3}\right) \end{aligned} \tag{7}$$

where K_{emf} is the constant of the electromotive force and ω_e is the electric angular frequency. The electric equations of the PMSG are described by (8).

$$\begin{bmatrix} V_a \\ V_b \\ V_c \end{bmatrix} = -R_{Lga}\begin{bmatrix} i_a \\ i_b \\ i_c \end{bmatrix} - L_{ga}\frac{d}{dt}\begin{bmatrix} i_a \\ i_b \\ i_c \end{bmatrix} + \begin{bmatrix} e_a \\ e_b \\ e_c \end{bmatrix} \tag{8}$$

Analyzing the behavior of the PMSG, it is obtained that the electromotive torque (T_e) is determined by (9)

$$T_e = \frac{3K_{emf}I_g}{2\sqrt{2}} \tag{9}$$

where I_g is the generator phase rms current.

3. Modelling Wind Generation System

The main goal in wind power generation system is to extract the greatest amount of wind energy and convert it to electric energy. This is achieved with an appropriate algorithm of the Maximum Power Point Tracking (MPPT) and adequate control structure that allows the system to be stable in the range of operation. Whereas the mechanical power of the turbine (P_{mec}) is equal to the electric power generator or generator output power (P_{out}), as shown in (10).

$$P_{mec} = T_{ind}\omega_m = P_{out} \tag{10}$$

Considering the electrical losses of the generator and the torque induced in the turbine is equal to the electrical torque in the generator. The generator output power is expressed by

$$P_{out} = T_e\omega_m - R_{Lga}I_g \tag{11}$$

Applying (9) in (11), it is obtained:

$$P_{out} = \frac{3K_{fem}}{\sqrt{2}}I_g\omega_m - R_{Lga}I_g \tag{12}$$

Because of the power function is not linear, a linear model of P_{out} may be obtained by applying a first order Taylor series around the operation point. This linear model allows a small-signal analysis to determine which system is most suitable control.

$$\hat{P}_{out} = \hat{\omega}_m \frac{\partial\left[P_{out}(\omega_m, i_g)\right]}{\partial \omega_m}\bigg|_{\substack{\omega_m = W_m \\ i_g = I_g}} + \hat{\imath}_g \frac{\partial\left[P_{out}(\omega_m, i_g)\right]}{\partial i_g}\bigg|_{\substack{\omega_m = W_m \\ i_g = I_g}} \tag{13}$$

Developing, it is obtained

$$\hat{P}_{out} = \hat{\omega}_m \frac{3K_{fem}}{\sqrt{2}} I_g + \hat{\imath}_g \left(\frac{3K_{fem}}{\sqrt{2}} W_m - R_{Lga} I_g\right) \tag{14}$$

From (14), the analysis can be performed to select which of the two structures is the most appropriate control for this WGS. By (14), it is shown that the generator output power has a dependence of both the generator current and the generator speed, which is shown in Fig. 5.

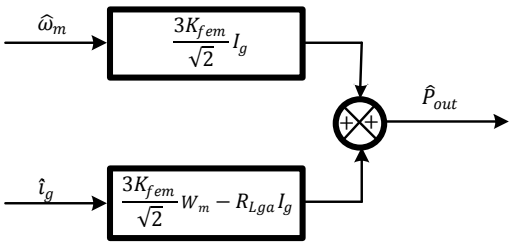

Fig. 5. Dependence of the generator output power $(\hat{P}_{out})$.

To analyze the two control structures in the WPGS, it is needed to obtain the dependence of the power function of a single variable. If the control structure is analyzed through the torque, it is needed to obtain the relationship between the generator output power and generator torque $(\hat{P}_{out}/\hat{T}_e)$ or the relationship between the generator output power and generator current$(\hat{P}_{out}/\hat{\imath}_g)$, as shown in Fig. 6, because the generator torque has a direct relationship with the current generator as shown in (9). If the control structure is analyzed through the generator speed, it is needed to obtain the relationship between the generator output power and generator speed $(\hat{P}_{out}/\hat{\omega}_m)$, as shown in Fig. 7.

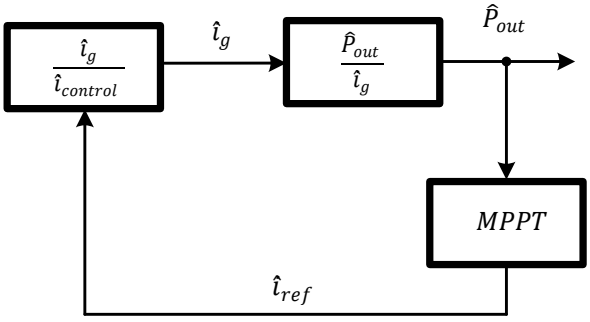

Fig. 6. The basic block diagram of torque control structure in the wind generator system.

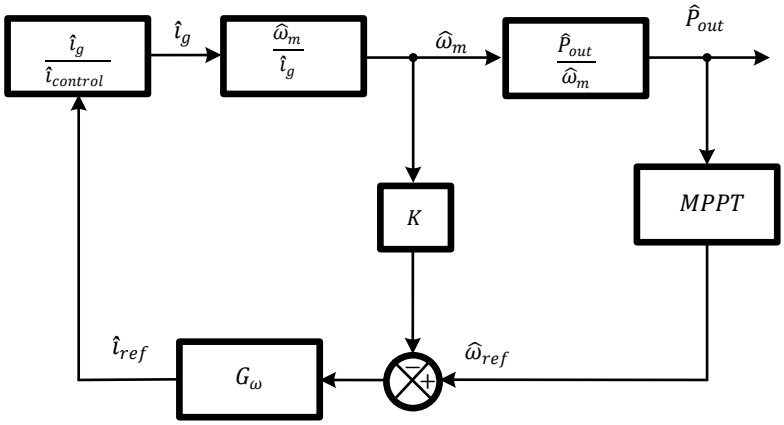

Fig. 7. The basic block diagram of speed control structure in the wind generator system.

To analyze the torque control structure, it is necessary to obtain the relationship between generator output power and generator current $(\hat{P}_{out}/\hat{\imath}_g)$. Starting from equation (14), it is obtained (15). In (15) is observed that $\hat{P}_{out}/\hat{\imath}_g$ depends on the relationship generator speed and generator current $(\widehat{\omega}_m/\hat{\imath}_g)$.

$$\frac{\hat{P}_{out}}{\hat{\imath}_g} = \frac{\widehat{\omega}_m}{\hat{\imath}_g}\frac{3K_{fem}}{\sqrt{2}}I_g + \frac{3K_{fem}}{\sqrt{2}}W_m - 2R_{Lga}I_g \tag{15}$$

To analyze the speed control structure, it is necessary to obtain the relationship between generator output power and generator speed $(\hat{P}_{out}/\widehat{\omega}_m)$. Starting from equation (14), it is obtained (16). It is also necessary to implementing a speed control loop to complete the control structure. In (16) is observed that $\hat{P}_{out}/\hat{\imath}_g$ depends on the relationship generator current and generator speed $(\hat{\imath}_g/\widehat{\omega}_m)$.

$$\frac{\hat{P}_{out}}{\widehat{\omega}_m} = \frac{3K_{fem}}{\sqrt{2}}I_g + \frac{\hat{\imath}_g}{\widehat{\omega}_m}\left(\frac{3K_{fem}}{\sqrt{2}}W_m - 2R_{Lga}I_g\right) \tag{16}$$

In both structures, it is necessary to know the relationship generator speed and generator current. Starting from equation (1), it is obtained (17). The following nomenclature is adopted: any dynamic variable *x* is represented as: $= X + \hat{x}$, where *X* is the operation point value and $\hat{x}$ is the small-signal term.

$$\omega_m = \frac{1}{Js}(T_m - T_e) \tag{17}$$

T_m is normally considered an internal disturbance in the system. However, T_m strongly depends on both the speed of the PMSG, ω_m, and the wind speed, v_ω, as it is shown in (3)-(6). T_e depends on the I_g as shown in (9).Therefore, in this paper include Tm, so considering all the variables involved in the system, which allows a complete analysis of the system. Fig. 8 shows the block diagram of modeling the mechanical behavior of wind generation system.

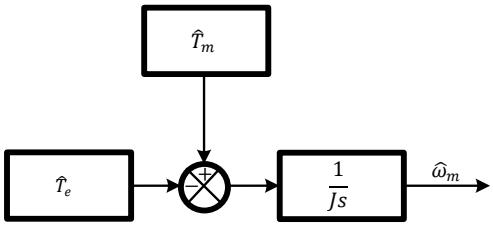

Fig. 8. Diagrama de bloques básico del modelo del comportamiento mecánico del SGE

Applying (4), (5) and (6) in (3), it is obtained:

$$T_m = \frac{1}{2}\rho\pi r^3\left(\frac{a v_\omega}{r\omega_m} + b + \frac{cr\omega_m}{v_\omega} + \frac{dr^2\omega_m^2}{v_\omega^2} + e\frac{r^3\omega_m^3}{v_\omega^3} + f\frac{r^4\omega_m^3}{v_\omega^4}\right) v_\omega{}^2 \tag{18}$$

Because of the T_m is not linear, a linear model of T_m may be obtained by applying a first order Taylor series around the operation point. Note that one of the inputs of the resulting linear model is the wind speed, which is considered as an external disturbance, and the other one is the inherent feedback of the generator speed.

$$\hat{T}_m = \hat{\omega}_m \left.\frac{\partial[T_m(\omega_m, v_\omega)]}{\partial\omega_m}\right|_{\substack{\omega_m=W_m \\ v_\omega=V_\omega}} + \hat{v}_\omega \left.\frac{\partial[T_m(\omega_m, v_\omega)]}{\partial v_\omega}\right|_{\substack{\omega_m=W_m \\ v_\omega=V_\omega}} \tag{19}$$

Developing, it is obtained

$$\begin{aligned}\hat{T}_m = {} & \frac{1}{2}\rho\pi r^3\left(-\frac{aV_\omega^3}{rW_m^2} + crV_\omega + 2dr^2W_m + \frac{3er^3W_m^2}{V_\omega} + \frac{4fr^4W_m^3}{V_\omega^2}\right)\hat{\omega}_m \\ & + \frac{1}{2}\rho\pi r^3\left(\frac{3aV_\omega^2}{rW_m} + 2bV_\omega + crW_m - \frac{er^3W_m^3}{V_\omega^2} - \frac{4fr^4W_m^4}{2V_\omega^3}\right)\hat{v}_\omega\end{aligned} \tag{20}$$

As the wind speed is an external disturbance, $\hat{v}_\omega = 0$ is considered to analyze the stability of the speed control loop. The small-signal term of T_m is expressed by (21).

$$\hat{T}_m\big|_{\hat{v}_\omega=0} = \frac{1}{2}\rho\pi r^3\left(-\frac{aV_\omega^3}{rW_m^2} + crV_\omega + 2dr^2W_m + \frac{3er^3W_m^2}{V_\omega} + \frac{4fr^4W_m^3}{V_\omega^2}\right)\hat{\omega}_m \tag{21}$$

Therefore, the small-signal expression of the electrical torque may be obtained from (9), resulting in (22).

$$\hat{T}_e = \frac{3K_{fem}\hat{\imath}_g}{\sqrt{2}} \tag{22}$$

Considering that there are not variations in wind speed, $\hat{v}_\omega = 0$, the PMSG speed is expressed by (23). Fig. 9 shows the block diagram modeling the mechanical behavior of wind generation systems, considering the wind speed, the speed of the generator and the generator current.

$$\hat{\omega}_m = \frac{1}{Js}\left(\hat{T}_m\big|_{\hat{v}_\omega=0} - \hat{T}_e(i_g)\right) \tag{23}$$

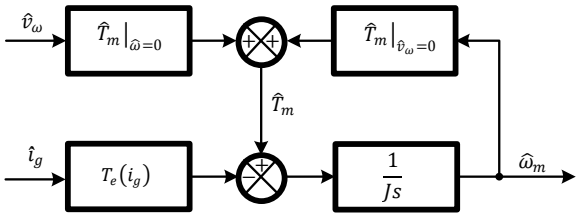

Fig. 9. Block diagram of the model the mechanical behavior of WGS, considering the variables involved.

From (21)-(23), it is obtained

$$\widehat{\omega}_m = \frac{1}{Js}\left[\frac{1}{2}\rho\pi r^3\left(-\frac{aV_\omega^3}{rW_m^2} + crV_\omega + 2dr^2W_m + \frac{3er^3W_m^2}{V_\omega} + \frac{4fr^4W_m^3}{V_\omega^2}\right)\widehat{\omega}_m - \frac{3K_{fem}\hat{\imath}_g}{\sqrt{2}}\right] \quad (24)$$

From the equation (24), it is possible to deduce the relationship between the PMSG speed and generator current, it is expressed by

$$G_{\omega g}(s) = \frac{\widehat{\omega}_m}{\hat{\imath}_g} = -\frac{3K_{fem}}{\sqrt{2}\left[Js - \frac{1}{2}\rho\pi r^3 c_1\right]}$$
$$c_1 = \left(-\frac{aV_\omega^3}{rW_m^2} + crV_\omega + 2dr^2W_m + \frac{3er^3W_m^2}{V_\omega} + \frac{4fr^4W_m^3}{V_\omega^2}\right) \quad (25)$$

Fig. 10 shows the Bode diagrams of the relationship between the PMSG speed and generator current $(\widehat{\omega}_m/\hat{\imath}_g)$ to V_ω = 10 m/s, as a function of λ.

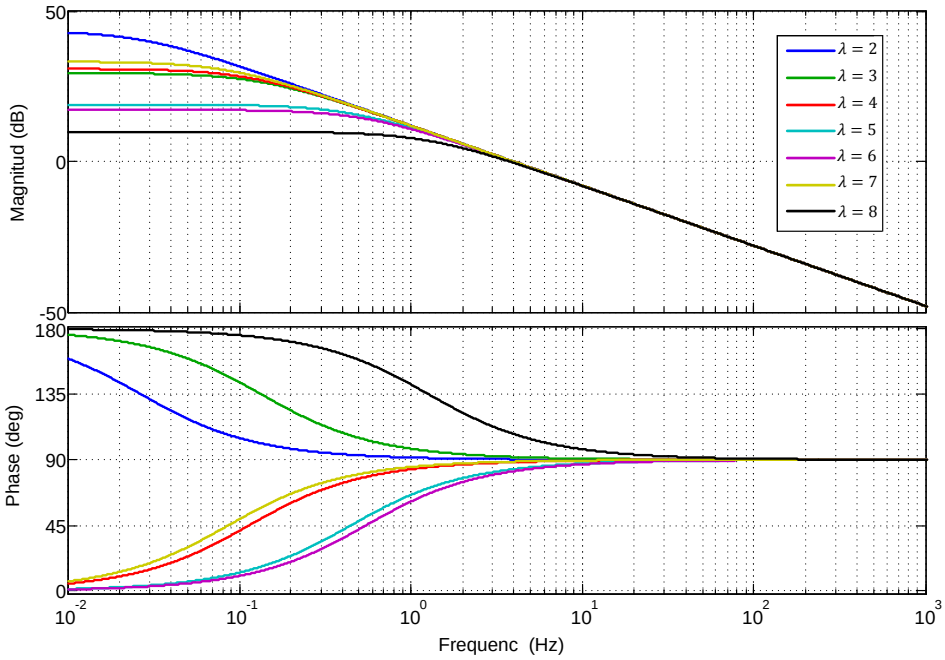

Fig. 10. Bode diagrams of the relationship between the PMSG speed and generator current $(\widehat{\omega}_m/\hat{\imath}_g)$ to V_ω = 10 m/s, as a function of λ.

4. Torque Control vs Speed Control

In order to determine which control structure is the most suitable for use in the proposed wind generation system. It is necessary to obtain $\hat{P}_{out}/\hat{\imath}_g$ to analyze the torque control and $\hat{P}_{out}/\widehat{\omega}_m$ to analyze the speed control.

Analyzing the torque control structure, it is substituted (25) in (15), obtaining the transfer function from the generator current to generator output power, it is expressed by

$$\frac{\hat{P}_{out}}{\hat{\imath}_g} = \frac{-9{K_{fem}}^2 I_g + \left(\frac{3K_{fem}}{\sqrt{2}}W_m - 2R_{Lga}I_g\right)[2Js - \rho\pi r^3 c_1]}{[2Js - \rho\pi r^3 c_1]} \quad (26)$$

$$c_1 = \left(-\frac{aV_\omega^3}{rW_m^2} + crV_\omega + 2dr^2W_m + \frac{3er^3W_m^2}{V_\omega} + \frac{4fr^4W_m^3}{V_\omega^2} \right)$$

Fig. 11 shows Bode diagrams of the transfer function from the generator current to generator output power $(\hat{P}_{out}/\hat{\imath}_g)$ to V_ω = 10 m/s, as a function of λ.

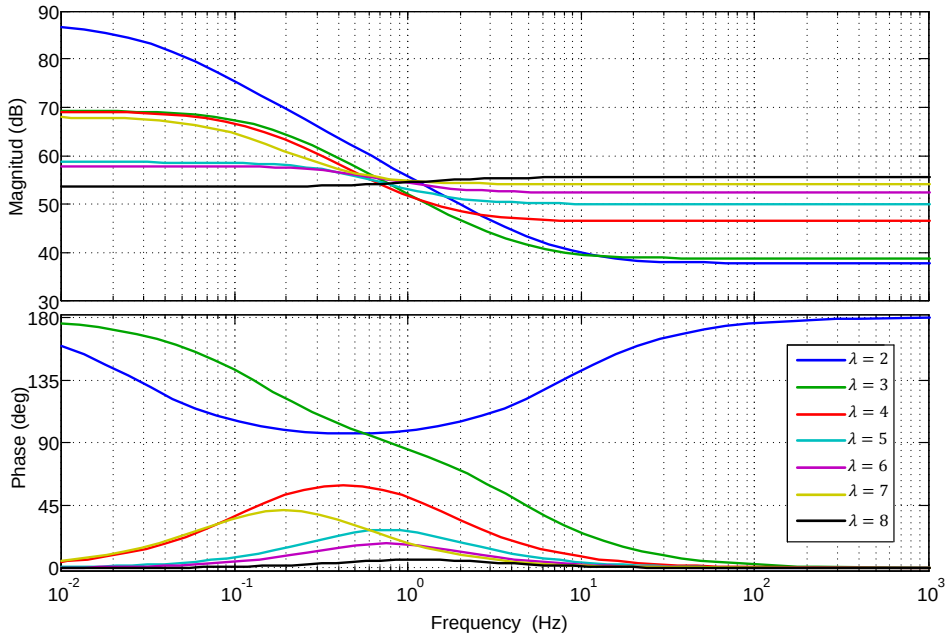

Fig. 11. Bode diagrams of the transfer function from the generator current to generator output power $(\hat{P}_{out}/\hat{\imath}_g)$ to V_ω = 10 m/s, as a function of λ.

Fig. 11 shows that $\hat{P}_{out}/\hat{\imath}_g$ is unstable for λ values greater than 3. This is corroborated in Fig. 12, which shows the location of the roots of $\hat{P}_{out}/\hat{\imath}_g$, for λ values between 4 and 7; note that the poles and zeros are in the right half plane at very low frequency and very close to each other for different operating points. This allows to establish that torque control structure is very complicated to implement using classical control theory.

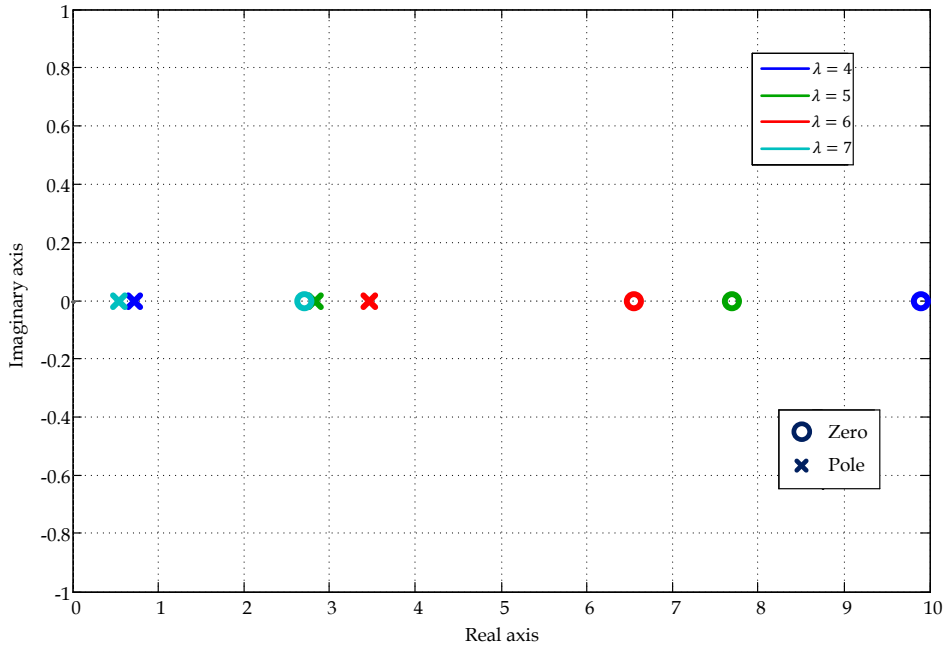

Fig. 12. Location of the roots of the transfer function from the generator current to generator output power $(\hat{\boldsymbol{P}}_{\boldsymbol{out}}/\hat{\boldsymbol{\imath}}_{\boldsymbol{g}})$ to $\boldsymbol{V_\omega}$ = 10 $\boldsymbol{m/s}$, as a function of λ.

Analyzing the torque control structure, it is substituted (25) in (16), obtaining the transfer function from the generator speed to generator output power, it is expressed by

$$\frac{\hat{P}_{out}}{\hat{\omega}_m} = \frac{3K_{fem}}{\sqrt{2}} I_g - \left(W_m - \frac{2\sqrt{2}R_{Lga}I_g}{3K_{fem}} \right) \left[Js - \frac{1}{2}\rho\pi r^3 c_1 \right]$$
$$c_1 = \left(-\frac{aV_\omega^3}{rW_m^2} + crV_\omega + 2dr^2W_m + \frac{3er^3W_m^2}{V_\omega} + \frac{4fr^4W_m^3}{V_\omega^2} \right) \quad (27)$$

Fig. 13 shows Bode diagrams of the transfer function from the generator speed to generator output power $(\hat{P}_{out}/\hat{\omega}_m)$ to V_ω = 10 m/s, as a function of λ.

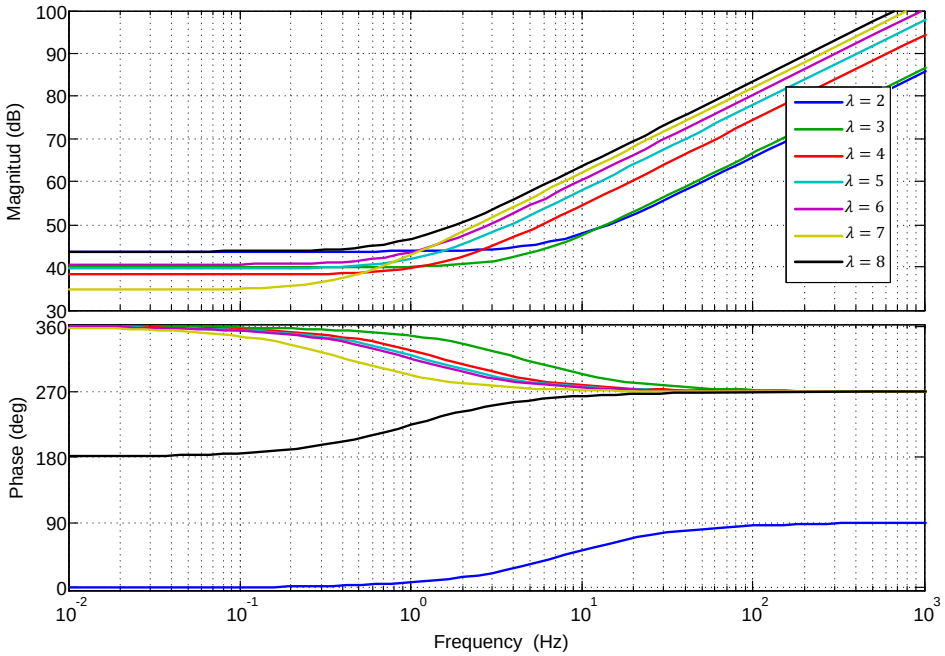

Fig. 13. Bode diagrams of the transfer function from the generator speed to generator output power $(\hat{\boldsymbol{P}}_{\boldsymbol{out}}/\hat{\boldsymbol{\omega}}_{\boldsymbol{m}})$ to $\boldsymbol{V_\omega}$ = 10 $\boldsymbol{m/s}$, as a function of λ.

Fig. 13 shows that $\hat{P}_{out}/\hat{\omega}_m$ is non-minimum phase system, because contains zeros in the right half plane, for various values of λ. This allows to establish that speed control structure can be implemented using classical control techniques.

5. Implementation of the Structure Speed Control

5.1 AC/DC Converter and Current Control Loop

The AC/DC converter employee is a Three-Phase Boost Rectifier operating in Discontinuous Conduction Mode (DCM) with Peak Current Mode Control (PCC), this was presented in [15], where it was presented and analyzed in detail. The Boost Rectifier operating in DCM achieves a Total Harmonics Distortion (THD_i) of the generator currents, much lower than that achieved by the same topology operating in Continuous Conduction Mode (CCM), improving the power factor of the generator [17]. In the current paper it is only presented the most relevant issues to assess the speed control structure in the proposed wind generation system. Fig. 14 shows the Three-Phase Boost rectifier operating in DCM with PCC.

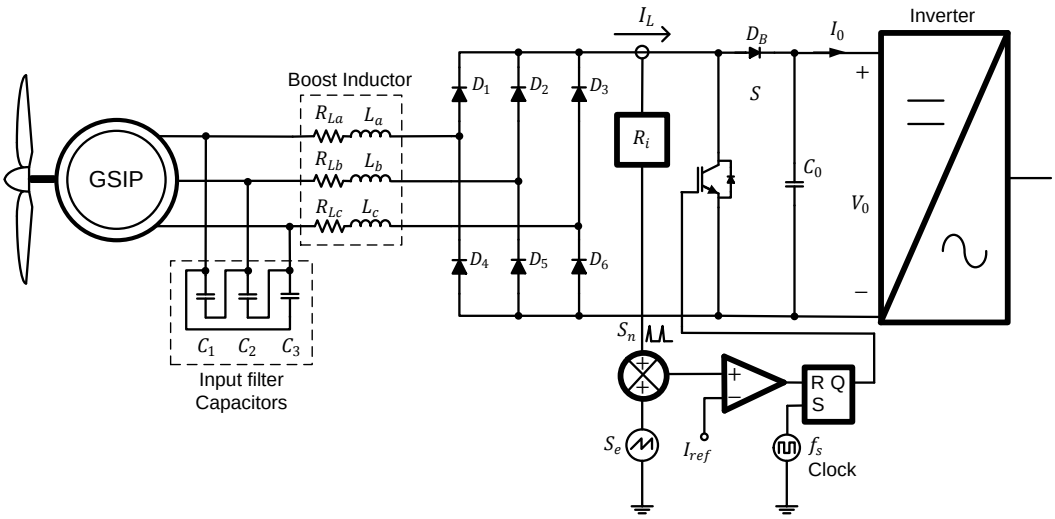

Fig. 14. Three-Phase Boost rectifier operating in DCM with PCC.

$G_{id}(s) = \hat{\imath}_L(s)/\hat{d}(s)$ is the transfer function from the duty cycle to the equivalent boost inductor current, expressed by (28).

$$G_{id}(s) = \frac{\hat{\imath}_L(s)}{\hat{d}(s)} = \frac{-\left(s^2 C_i L_g + s C_i R_g + 1\right)(K_i + K_o)}{s^3 B_3 + s^2 B_2 + s B_1 + B_0}$$

$$B_3 = C_i L_g L\left(g_i + g_o + g_f\right)$$

$$B_2 = C_i\left[L_g + \left(g_i + g_o + g_f\right)\left(L R_{L_g} + L_g R_L\right)\right] \tag{28}$$

$$B_1 = \left[C_i R_{L_g} + \left(g_i + g_o + g_f\right)\left(L_g + L + C_i R_L R_{L_g}\right)\right]$$

$$B_0 = \left(g_i + g_o + g_f\right)\left(R_{L_g} + R_L\right) + 1$$

where the values of the parameters of the PWM switch small-signal model in DCM [18] are shown in (29).

$$g_i = \frac{D^2}{2Lf_s} \qquad g_o = \frac{2LP_o^2 f_s}{D^2 V_i^2 V_o^2} \qquad g_f = \frac{2P_o}{V_i V_o}$$

$$K_i = -\frac{DV_i}{Lf_s} \qquad K_o = -\frac{2P_o}{DV_o} \tag{29}$$

In (28) and (29) it is considered: $L_g = 2L_{ga}$, $R_{Lg} = 2R_{Lga}$, $L = 2L_a$, $R_L = 2R_{La}$ and $C_i = 3C_{f1}/2$. D is the duty cycle of the boost active switch. V_i is the average value of the Boost DC-DC converter input voltage, as it is shown in Fig. 14. The boost rectifier output voltage, V_o, is regulated by the grid connected inverter to a constant value of *650V*. P_o is the output power at the operating point, which is limited to the maximum value allowed by the PMSG.

Fig. 15 shows the block diagram of the current loop with PCC [19]. The reference for the current loop, I_{ref}, is provided by the controller of the speed control loop.

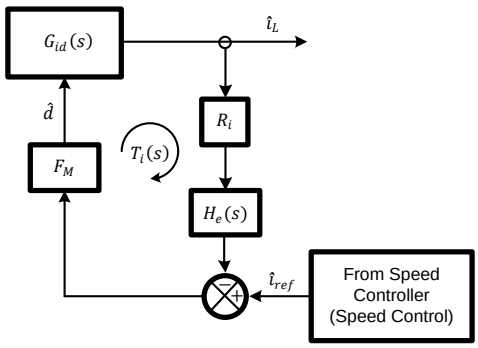

Fig. 15. Peak Current-Mode Control Loop.

The loop gain of the current loop, $T_i(s)$, is determined by (30). $R_i = 0.015\ \Omega$ is the current sense gain, F_M is the PWM modulator gain, and $H_e(s)$ is the sampling gain [19], typical in peak current mode control.

$$T_i(s) = G_{id}(s)H_e(s)R_iF_M \tag{30}$$

The sampling gain $H_e(s)$ is expressed by (31)

$$H_e(s) = 1 + \frac{s}{\omega_z Q_z} + \frac{s^2}{\omega_z^2}$$

where

$$\omega_z = \frac{\pi}{T_s} = \frac{\pi}{200\mu s} = 15707.963\frac{rad}{s} \tag{31}$$

$$Q_z = -\frac{2}{\pi} = -0.6366$$

In order to guarantee the stability of the current loop, the PWM modulator gain, F_M, expressed by (32), should be adjusted properly.

$$F_M = \frac{1}{(S_n + S_e)T_s} \tag{32}$$

In (32) S_n is the on-time slope of the current sense waveform, S_e is the slope of the stabilization ramp, $Se\ =\ 22.503\ V/ms$. The value of S_n is obtained from (33).

$$S_n \approx \frac{V_i}{L}R_i \tag{33}$$

The closed loop gain of the current loop is given by

$$G_{ic}(s) = \frac{\hat{\imath}_L(s)}{\hat{\imath}_{ref}(s)} = \frac{G_{id}(s)F_M}{1 + T_i(s)} \tag{34}$$

As the PMSG torque depends on the generator currents, it is important to know the relationship between the generator current and the equivalent boost inductor current, following (35).

$$\frac{\hat{\imath}_g(s)}{\hat{\imath}_L(s)} = \frac{1}{s^2C_iL_g + sC_iR_{Lg} + 1} \tag{35}$$

Table II shows the values of its most relevant parameters.

Table II. Characteristics in the Three-Phase Boost rectifier operating in DCM with PCC.

Characteristics	Values
Boost Inductance associated to each phase ($L_a, L_b, L_c = L/2$)	$375\ \mu H$
Resistance in series associated to the Boost inductor in each phase (R_{La}, R_{Lb}, R_{Lc})	$37.5\ m\Omega$.
Capacitance of the filter (C_1, C_2, C_3)	$2.2\ \mu F$
Current sense gain (R_i)	$0.015\ \Omega$.
Slope of the stabilization ramp (S_e)	$22.503\ V/ms$

5.2 Speed Control Loop

Once set the AC / DC converter used in the WGS, it is performed small-signal analysis of the system around the operating point and it is developed the speed loop for the system is stable to variations in generator speed.

This analysis of the dynamics of the turbine expressed by (17), considering the mechanical torque developed in (21) and the electric torque depends on the generator current expressed in (22), the current control loop, which includes Boost-phase rectifier and input filter represented in (34) and (35), respectively, Fig. 16 shows the block diagram of the speed control loop.

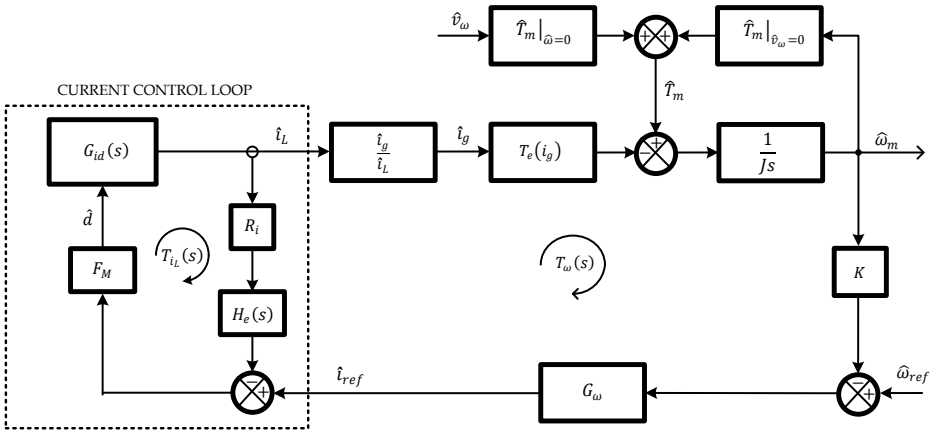

Fig. 16. Block diagram of the speed control loop

where $K = 1$ is the speed sensing gain, G_ω is the transfer function of a simple proportional-integral controller and ω_{ref} is the reference speed loop, which is provided by a search algorithm for maximum power point, which is outside the scope of this paper.

To analyze the response of the system, wind speed is considered a disturbance input of the system, which provides that $\hat{v}_\omega = 0$, so that the relationship between speed generator and current generator is expressed by (25), also the current loop is reduced to that expressed in (34), the block diagram of the speed loop can be reduced to that shown in Fig. 17.

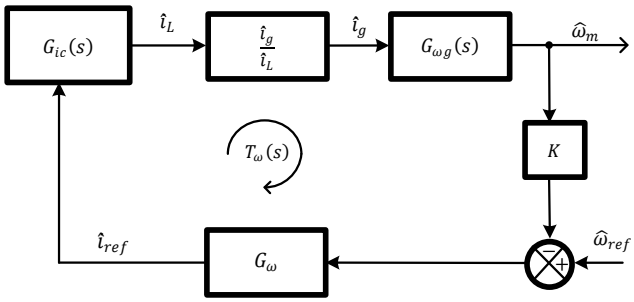

Fig. 17. Block diagram of speed control loop reduced.

The loop gain of the speed loop, $T_\omega(s)$, is determined by (36).

$$T_\omega(s) = G_{ic}(s)G_{\omega g}(s)\frac{\hat{\imath}_g(s)}{\hat{\imath}_L(s)}KG_\omega(s) \tag{36}$$

The chosen gains for the PI speed controller, G_ω , are: K_p=*–0.05777* and K_i=*–0.0187752 rad/s.* The closed loop transfer function from the reference speed to the PMSG speed is given by (37). Fig. 18 shows the Bode diagrams of T_ω with the chosen controller.

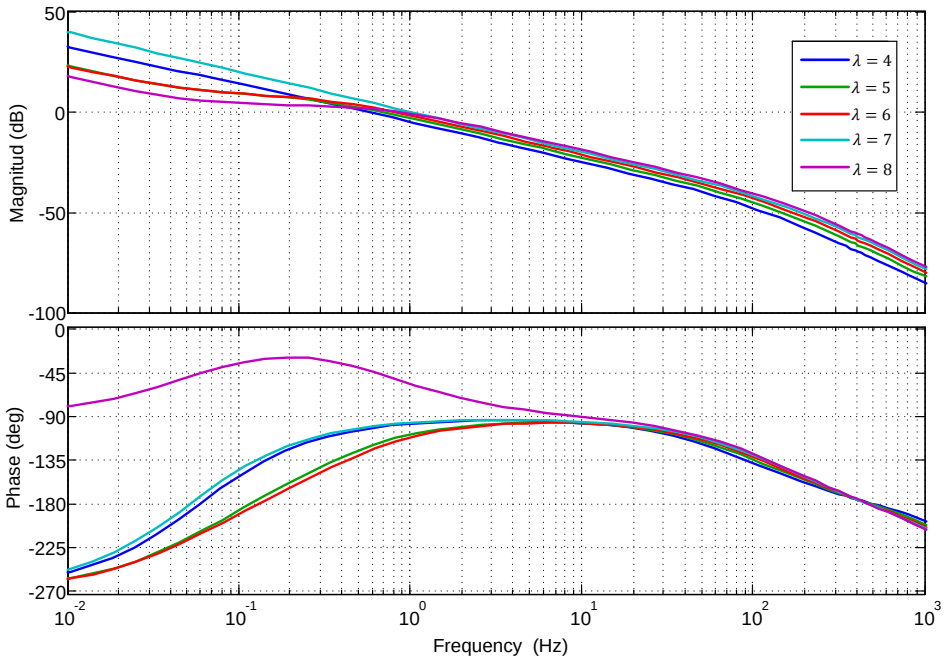

Fig. 18. Bode diagram of the speed loop gain $T_\omega(s)$, at a wind speed of 6 m/s

The transfer function of the speed control in closed loop is determined by (38) and it is shown in Fig. 19.

$$G_{\omega r} = \frac{\widehat{\omega}_m}{\widehat{\omega}_{ref}} = \frac{G_{ic}(s)G_{\omega g}(s)\frac{\hat{\imath}_g(s)}{\hat{\imath}_L(s)}G_\omega(s)}{1 + T_\omega} \tag{37}$$

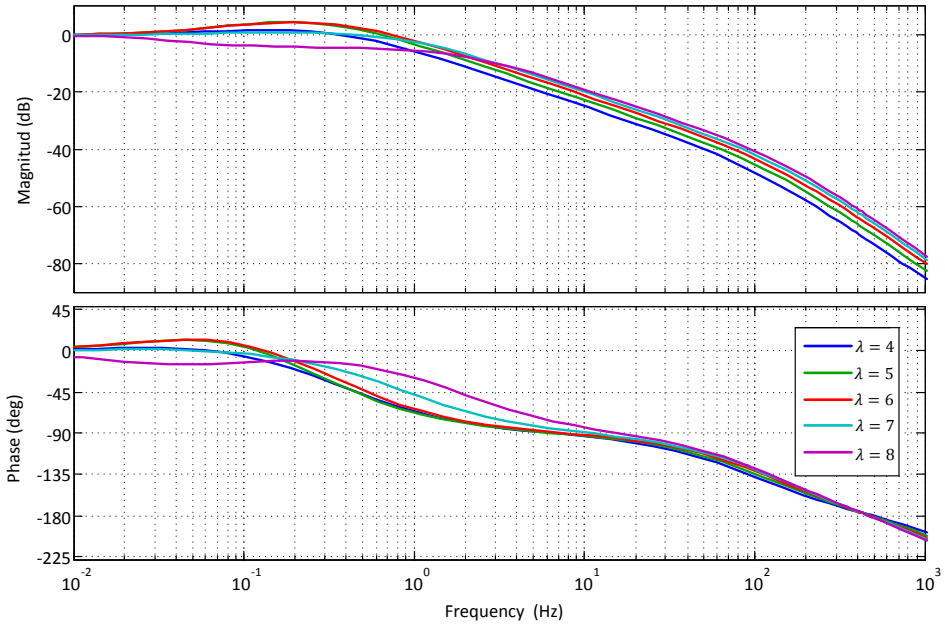

Fig. 19. Bode diagram of transfer function of the speed control loop closed, $G_{\omega r}(s)$, at a wind speed of 6 m/s.

5.3 Speed estimator

To obtain the feedback signal for the speed control loop, it is possible to mount speed sensors on the shafts of the PMSG (resolvers, encoders or Hall-effect sensors). However, the use of these sensors increases the complexity, weight and cost of PMSG.

As both the voltages and frequency of the generator depend on its speed, the PMSG speed can be estimated starting from the measurement of the electrical quantities, eliminating the need for mechanical sensors. The problem is that the measured signals contain low frequency harmonics of the fundamental frequency of the generator, as well as switching frequency components due to the boost rectifier. Furthermore, the fundamental and its low frequency harmonics have different values depending on the generator speed. These issues have been studied in [21], concluding that the use of a Linear Kalman Filter (LKF) is a good compromise among dynamical response, static performance and complexity of implementation. In this case sensors are used to measure the generator output voltages in order to apply the LKF speed estimation. The main equations of the LKF used in this work are expressed by (38). The meaning of each variable of (38) in explained in [21].

$$\begin{aligned} \varepsilon(k) &= V_\beta(k)\cos\theta(k) - V_\alpha(k)\sin\theta(k) \\ \theta(k+1) &= \theta(k) + T_s\omega_e(k) + K_{s1}\varepsilon(k) \\ \omega_e(k+1) &= \omega_e(k) + \acute{\rho}(k) + K_{s2}\varepsilon(k) \\ \acute{\rho}(k+1) &= \acute{\rho}(k) + K_{s3}\varepsilon(k) \end{aligned} \tag{38}$$

The chosen values of the LKF parameters are: δ=5x10^6, $K_{s1} = 0.0032896$, $K_{s2} = 0.54221$ and $K_{s3} = 0.00044647$. It is worth pointing out that the LKF gains are independent of the PMSG parameters and could be used with a different generator. Another advantage of the LKF speed estimator is that the only measurement needed is that of the output voltages of the PMSG, reducing the cost of the sensors in the system.

6 Results

Fig. 20 shows the scheme of the proposed WECS. The performance of the proposed WECS has been evaluated by means of PSIM 7.0.5 software [20]. The system includes Boost rectifier in DCM with input filter and control PCC, the wind turbine model, the sensing speed by a speed estimator and the speed loop through the controller designed.

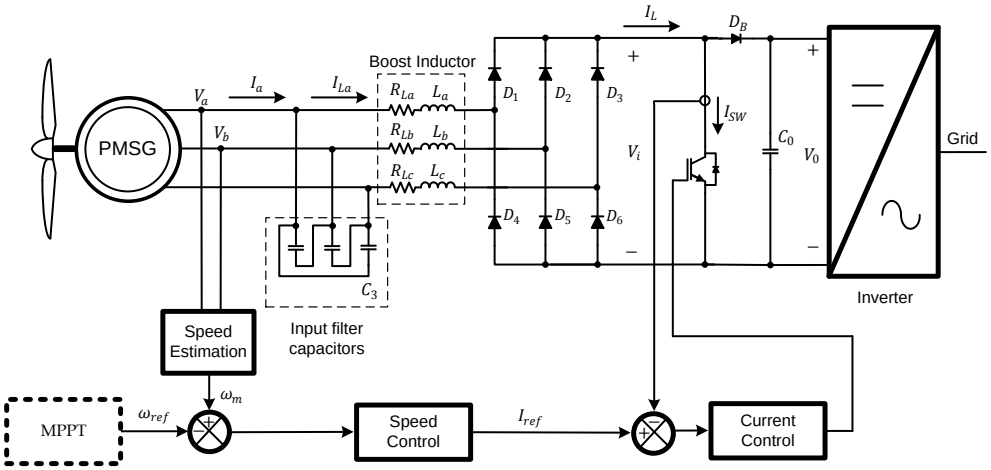

Fig. 20. Scheme of the proposed WGS.

In order to evaluate whether the speed control structure is adequate in the WGS, steps are applied in the reference speed to observe the behavior of the WGS, with constant wind speed. The steps $(\Delta\omega_{ref})$ are 20 rpm, the update time (Δt) of the reference is 10s and the wind speed is 6 m/s, 10 m/s and 10 m/s. The reference speed starts at 150 rpm, however, the WGS is limited to a maximum reference speed, according to the behavior of the turbine, so for the case of 6 m/s, maximum speed is 310 rpm; for 6 m/s, it is 430 rpm; and for 6 m/s, it is 530 rpm.

Fig. 21 shows the behavior of the speed loop to steps in the speed reference at a constant wind speed of 6 m/s. Fig. 22 shows the behavior of the speed loop to steps in the speed reference at a constant wind speed of 8 m/s. Fig. 23 shows the behavior of the speed loop to steps in the speed reference at a constant wind speed of 10 m/s. It is observed that the speed loop properly follows the reference value. Figures also show the behavior of the electric torque and the PMSG output power. It is observed that the speed loop properly follows the reference value in all case.

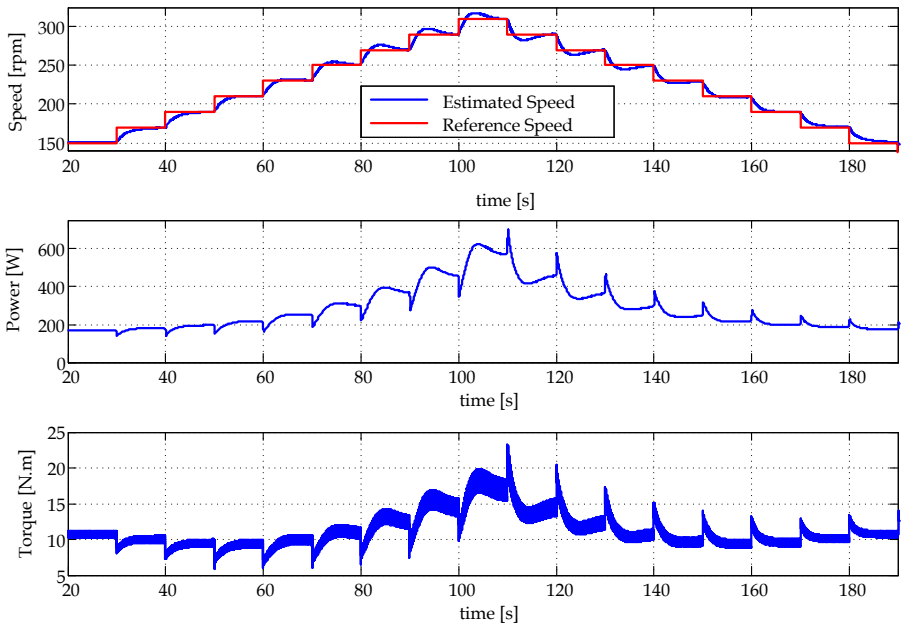

Fig. 21. Response of the speed loop to speed reference steps at a wind speed of 6 m/s. Top: generator speed and its reference. Middle: Generator output power. Bottom: Electric torque.

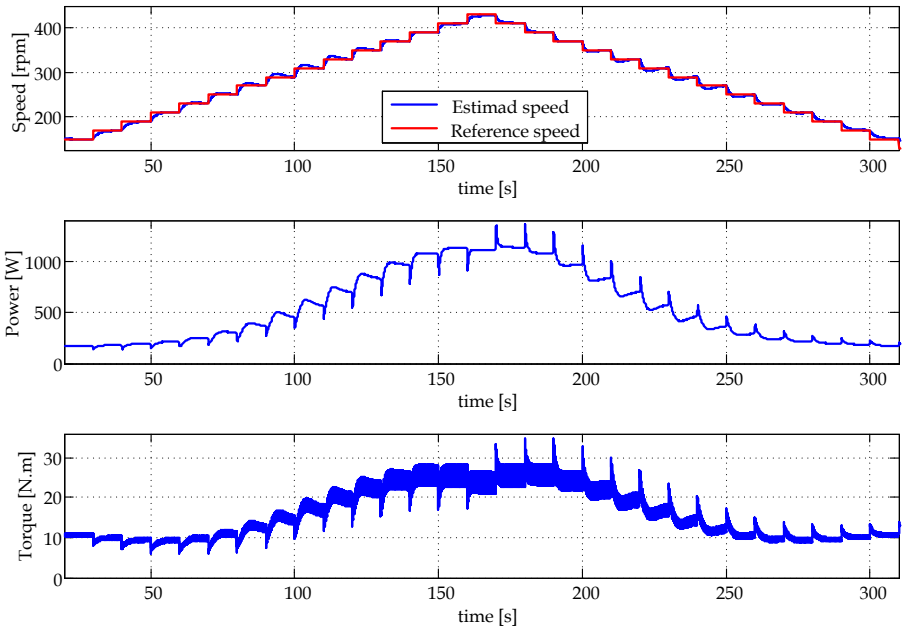

Fig. 22. Response of the speed loop to speed reference steps at a wind speed of 8 m/s. Top: generator speed and its reference. Middle: Generator output power. Bottom: Electric torque.

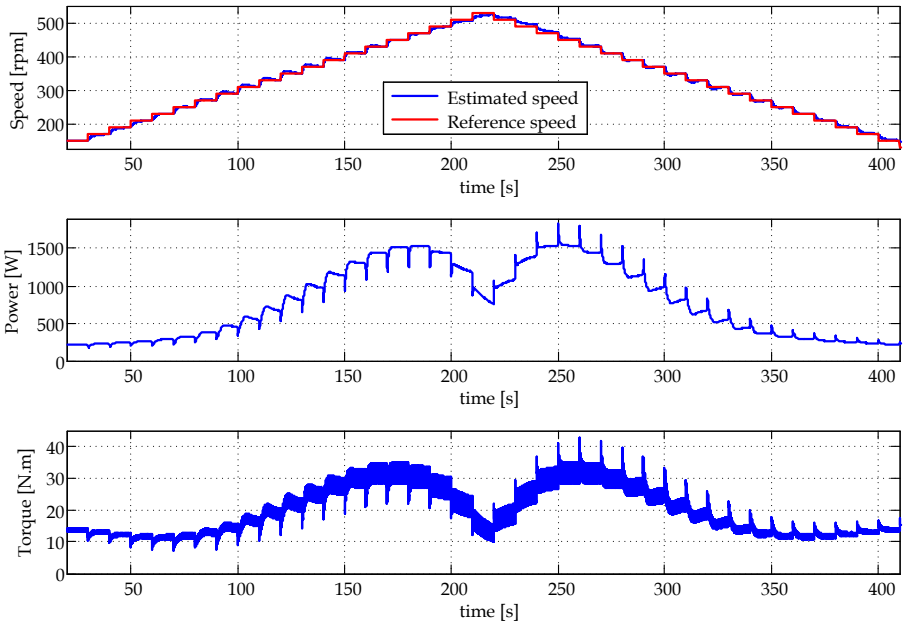

Fig. 23. Response of the speed loop to speed reference steps at a wind speed of 10 m/s. Top: generator speed and its reference. Middle: Generator output power. Bottom: Electric torque.

Fig. 24, Fig. 25 and Fig. 26 show in detail the speed loop response to steps in the reference speed, which is observed as for the speed loop always follow the setpoint established by the reference speed, regardless of wind speed and whether the reference speed increase or decrease, thereby demonstrating the speed control structure is adequate in the wind generation system.

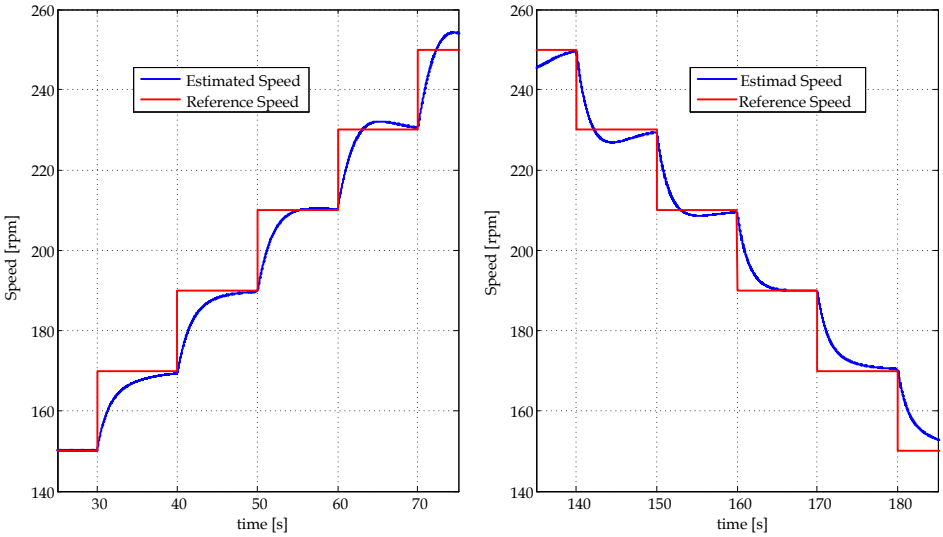

Fig. 24. Detail of the speed loop response to steps of the reference speed, a wind speed of $6\ m/s$

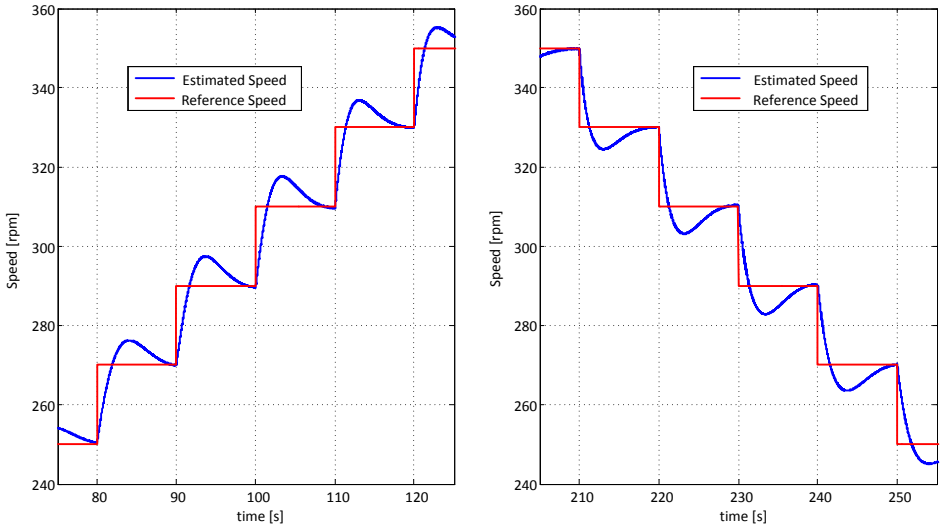

Fig. 25. Detail of the speed loop response to steps of the reference speed, a wind speed of $8\ m/s$

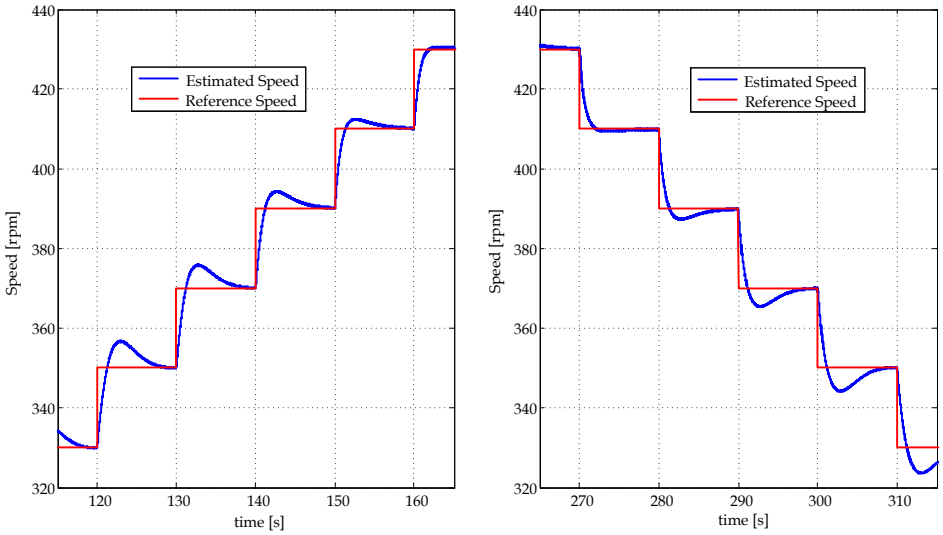

Fig. 26. Detail of the speed loop response to steps of the reference speed, a wind speed of $6\ m/s$

7 Conclusion

Analysis of the control structures in wind power generation system was concluded that the speed control is best suited for implementation because it is a nonminimum phase system, which can be

controlled by classical control theory, compared with the control of torque, which has poles and zeros in the right half plane, very low frequency and very close to each other, so it is very difficult to control using classical control theory.

The analysis of control structures considered all the elements of wind power generation system, taking great care of the turbine model, which considers the mechanical torque as a system variable and not as in other studies is considered as a perturbation internal system. Furthermore the analysis of the control structure is developed to be independent of the converters used on the system.

The implementation of wind power generation system for checking that the control structure is the most appropriate speed for this system, let to observe how the speed loop response to variations in the reference speed and how it stabilizes. In implementing the control structure is used a Three-phase rectifier Boost in DCM with an input filter and a PCC.

Acknowledgements

The first author thanks the support of the Instituto Politécnico Nacional (IPN) and of the Comisión de Operación y Fomento de Actividades Académicas (COFAA). This work was supported by the Spanish Ministry of Science and Innovation under Grant ENE2009-13998-C02-02.

References

[1] H. Li and Z. Chen, "*Overview of different wind generator systems and their comparisons*", IET Renewable Power Generation, Vol. 2, No. 2, pp. 123-138, June 2008.
[2] Fawzi A.L. Jowder, "Wind power analysis and site matching of wind turbine generators in Kingdom of Bahrain", Applied Energy 86 (4), pp. 538-545, April 2009.
[3] Brian Snyder, Mark J. Kaiser, *"A comparison of offshore wind power development in Europe and the U.S.: Patterns and drivers of development",* Applied Energy 86 (10), pp. 1845-1856, October 2009.
[4] Hannes Weigt, *"Germany's wind energy: The potential for fossil capacity replacement and cost saving"*, Applied Energy 86 (10), pp. 1857-1863, October 2009.
[5] Patrick J. Luickx, Erik D. Delarue, William D. D'haeseleer, "Considerations on the backup of wind power: Operational backup", Applied Energy 85 (9), pp. 787-799, September 2008.
[6] C.L. Trujillo, D. Velasco, E. Figueres, G. Garcerá, "Analysis of active islanding detection methods for grid-connected microinverters for renewable energy processing", Applied Energy, 87 (11), pp. 3591-3605, November 2010.
[7] Toshiaki Kaneko, Akie Uehara, Tomonobu Senjyu, Atsushi Yona, Naomitsu Urasaki, "An integrated control method for a wind farm to reduce frequency deviations in a small power system", Applied Energy, 88, (4), pp. 1049-1058, April 2011.
[8] R. Ahshan, M.T. Iqbal, George K.I. Mann, "Controller for a small induction-generator based wind-turbine", Applied Energy 85 (4), pp. 218-227, April 2008.
[9] Thomas Ackermann, "Wind Power in Power Systems", England, Wiley, 2005.
[10] Jamal A. Baroudi, Venkata Dinavahi, Andrew M. Knight, "A review of power converter topologies for wind generators" Renewable Energy 32, pp. 2369-2385, 2007.
[11] M. Arifujjaman, M. T. Iqbal and J. E. Quaicoe, "Energy capture by a small wind-energy conversion system". Applied Energy 85 (1), pp. 41-51, 2008.
[12] E. Bossanyi, "The Design of closed loop controllers for wind turbines", Wind Energy, Vol. 3 No. 3, pp. 149-163, Sep 2000.
[13] F. D. Bianchi, H. De Battista, R. J. Mantz, "Wind Turbine Control Systems", Germany, Springer, 2007.
[14] Yin Ming, Li Gengyin, Zhou Ming, Zhao Chengyong, "Modeling of the Wind Turbine with a Permanent Magnet Synchronous Generator for Integration", IEEE Power Engineering Society General Meeting, 2007, 24-28 June 2007 pp. 1–6.

[15] O. Carranza, G. Garcerá, E. Figueres, L.G. González, “Peak current mode control of three-phase boost rectifiers in discontinuous conduction mode for small wind power generators”, *Applied Energy, 87 (8), pp. 2728-2736, August 2010.*
[16] Yin Ming, Li Gengyin, Zhou Ming, Zhao Chengyong, “Modeling of the Wind Turbine with a Permanent Magnet Synchronous Generator for Integration”, *IEEE Power Engineering Society General Meeting*, 2007, 24-28 June 2007 pp. 1–6.
[17] Ali M. Eltamaly, “Harmonics reduction of three-phase boost rectifier by modulating duty ratio”, Electric Power Systems Research 77, pp. 1425–1431, 2007.
[18] V. Vorperian, “Simplified analysis of PWM converters using model of PWM switch I and II” IEEE Trans. on Aerospace and Electronic Systems, vol. 26 (3), pp. 490-505, may 1990.
[19] R. B. Ridley, "A new, continuous-time model for current-mode control (power convertors)”, IEEE Trans. on Power Electronics, vol. 6, no. 2, pp. 271-280, April 1991.
[20] PSIM 7.0 User´s Guide (2006), Powersim Inc., March 2006.
[21] O. Carranza, E. Figueres, G. Garcerá, L.G. González, "Comparative Study of Speed Estimators with Highly Noisy Measurement Signals for Wind Energy Generation Systems", Applied Energy, Volume 88, (3), pp. 805-813, March 2011.